A Broadband Mechanically-Tuned Superconducting Cavity Design Suitable for the Fermilab Main Injector

Brian J. Vaughn

***Abstract*— Radio Frequency (RF) superconductivity has been a mainstay of accelerator science for decades. However, its benefits have yet to be applied to proton synchrotrons with demanding tuning requirements. For example, the Main Injector (MI), Fermilab's high-energy proton synchrotron, currently utilizes 20+ ferrite-loaded cavities for a targeted 1.2 s acceleration cycle. Harnessing the extremely high gradients associated with superconductivity, the required number of cavities could be reduced by an order of magnitude, dramatically lowering operational power requirements even with cryogenic considerations. Additionally, the current plans for the Fermilab Accelerator Complex Evolution (ACE) initiative involve almost doubling the number of cavities in MI if the same designs are to be used, further highlighting the potential benefits of superconductivity. These advantages are attractive, but to date, no tunable superconducting cavity suitable for MI has been proposed due to the incompatibility of conventional broadband tuning methods with superconductivity. Here, we present a tunable superconducting cavity concept capable of record-breaking performance. Tuning will be accomplished by using high-speed linear actuators to vary the insertion depth of metallic plungers into the cavity volume. This tuning concept is theoretically viable with currently available technology and will be fully compatible with a superconducting cavity.**

***Index Terms*—Cavity Resonators, Proton Accelerators, Superconducting Devices, Tuners**

I. INTRODUCTION

RESEARCH efforts in particle accelerator physics are constantly pushing toward higher beam power. Fermilab is no exception, with the Accelerator Complex Evolution (ACE) initiative calling for a 2.3 MW upgrade of the lab's accelerator complex [1]. One phase of this initiative will focus on heavily modifying Fermilab's Main Injector (MI) such that it may achieve its 8-120 GeV acceleration cycle in roughly half of its current target 1.2 s cycle time, increasing the beam power proportionally. Right now, MI generates its accelerating gradient using 22 ferrite-loaded copper cavities. If the same cavity technology is to be used for ACE, current plans will increase that number to 37. While this strategy is technically feasible, the inefficiencies it presents are notable; this method will cause the RF loss within the cavities to quadruple relative to the current loss value if the shunt resistance is modified to keep the beam impedance in check (which is required for stable operation). This will drive up the operational electricity costs dramatically. Moreover, this method provides little wiggle-room to increase the beam intensity in the future, as the 37 cavities will perturb the beam substantially. These facts motivate consideration of alternative methods to achieve the necessary accelerating gradient.

In other accelerator applications, problems like this have been solved by reducing the required number of cavities using superconducting (SC) techniques. Using SC technology in the MI has the potential to lower the required gradient generation power dissipation by a factor of ~100. The MI, however, presents a challenge in this space, for no SC cavity design has been demonstrated that can handle both the required tuning speed and bandwidth of a MI cavity. Namely, the MI's cavities are currently able to tune between 52.813 MHz and 53.104 MHz, constituting a fractional bandwidth of ~.6 %. Again, this tuning range must be accessible within a time-scale on the order of 1 s.

Many examples of tunable SC cavities designs and implementations have been presented to date. At BNL's RHIC, a few tunable superconducting cavity concepts similar in frequency to an MI cavity have been created for storage rings [2], [3]. Cavities have also been developed that utilize ferro-electric tuners for microphonics compensation [4] or magnetostriction and thermal expansion for precision tuning [5]. Furthermore, the LHC exhibits a kHz tunable SC cavity [6]. An SC cavity concept oriented toward the Fermilab MI has even been conceptualized recently [7]. However, as stated above, these design techniques cannot meet the specifications of MI operation.

The ferro-electric implementation, for instance, functions based on the tuner's exceedingly low coupling to the cavity, resulting in a tuning range of less than 20 Hz and a power dissipation of 2.4 kW within the tuner for a 3 kW drive. While this is fast and precise for the use case in [4], scaling the tuner coupling to a level necessary to achieve the ~.6% fractional bandwidth MI tuning range would result in MW-level idle power dissipation within the tuner, negating the feasibility of this technique for the MI use case. It should be noted that ferrites would yield similar issues due to their loss tangents. The cavity design in [2], on the other hand, is a mechanical

This manuscript has been authored by Fermi Research Alliance, LLC under Contract No. DE-AC02-07CH11359 with the U.S. Department of Energy, Office of Science, Office of High Energy Physics.

B. J. Vaughn is with Fermi National Accelerator Laboratory, Batavia, IL, 60510, USA (e-mail: bvaughn@fnal.gov).

implementation that utilizes an actuator and flexible niobium membrane to vary the width of the quarter-wave cavity capacitive gap. While this solution is indeed innovative, it ultimately falls short of the MI requirements with a tuning bandwidth of ~.0873% at a tuning speed on the order of kHz/hr rather than kHz/s. The other SC cavity concept for the RHIC, specified in [3], appears to have the same deformation property and a similarly smaller, slower tuning range than is required for MI operation. Moreover, membrane/plate deformation is risky for a machine with a high cycle frequency, as a structural failure from metal fatigue would require expensive and time-consuming cavity repair and/or complete replacement. Similarly, the LHC 400 MHz cavity shows a .045% FBW using its pressure deformation-based tuning scheme, which is too small. The LEP fast tuner demonstrates high-speed tuning, as it is based on bias current magnetostriction of Ni rods that deform the cavities at millisecond timescales. However, again, this scheme is limited in terms of tuning range (~.000568%). The LEP slow thermal tuner exhibits a .0154% tuning range at 8 Hz/s, also insufficient. Finally, the MI-oriented concept demonstrated in [7], which uses and ancillary normal-conducting tunable resonator coupled to a static superconducting cavity to tune the resonance, demonstrates the speed requirement at a quoted 5 MHz/s, but does not have the necessary tuning range, capping at a .1% fractional bandwidth. Additionally, the cavity displays a relatively low unloaded Q on the order of 1×10^6 compared to typical SC cavity Q's, which routinely exceed 1×10^9.

From the above precedents, a mechanical solution could be a reasonable approach if the necessary speed, reliability, and tuning range can be achieved, but this will require a different technique from the ones presented above. This brings us to another tuning method that has been presented in [8]-[11]. This method depends on the insertion of a superconducting plunger into the cavity's electromagnetic volume, varying it and thus changing the cavity resonant frequency. While the plunger technique is not new, the potential of the technique is largely untapped in a manner not shared by the other methods discussed above. This is because a) the force required to move the plunger is small, unlike the mechanical schemes discussed above, which require many kN of constant force to achieve very small tuning ranges, b) long-term niobium cavity structural integrity is achievable since no niobium deformation is required, c) scaling the tuning metrics is conceptually simple, and d) the maximum speed is primarily limited by an external motor, which may be designed independently of the cavity.

In this paper, we will leverage the above advantages to expand the plunger technique, culminating in a feasibility study for a cavity design that may be implemented for use in the Fermilab Main Injector. The design presented herein will be shown to be able to meet the bandwidth and speed requirements of the MI without compromising gradient, unloaded Q, or any other metric relevant to SC cavity performance. The remainder of this paper will be organized as follows: in the next section, the topology, tuning mechanism, and performance of the cavity concept will be detailed. Then, the mechanical aspects of the tuning technique will be discussed. Finally, a multipacting study of the cavity geometry will be conducted.

II. Cavity Design Topology and Performance

In Fig. 1, a 3D model of the MI SC cavity concept, generated in CST Microwave Studio, is shown. The cavity uses a standard quarter-wave resonator geometry as a basis, much like in [2], but includes two niobium plungers at the shorted end. The plungers extend into niobium tubes terminated by flexible Inconel 625 edge-welded bellows to allow for linear motion in a sealed cavity (more on this in Section III). These bellows will ultimately interface through the helium bath to a linear actuation system outside the cryogenic assembly that varies the plunger insertion depth in the cavity. The effective electromagnetic volume of the cavity is tied to the plunger insertion depth. This tunes the resonant frequency. Both the plungers and cavity center conductor are hollow to support helium flow for convective cooling. To avoid shorts and scraping, the openings are large enough such that there is no physical contact between the plungers and cavity wall (a 5 mm clearance was chosen). The design also includes cylindrical sapphire windows that encase the plungers. Though they are not explicitly required and do marginally reduce the cavity Q (the tuning performance is unchanged), they add an extra layer of contamination protection without compromising the cavity Q, among other potential benefits that will be noted in the next section. The fin-like structures on the shorted endplate are for multipacting mitigation, as will be discussed in Section IV. The model is a simplified one, so the cryomodule, various mechanical elements, the external interfaces, and the linear actuators are not shown. Fig. 2 illustrates the plunger action. Since the plungers exit the cavity at the point of minimum tangential E-field, the energy coupling to the tubes is minor, even for large plungers, which increase tuner tube coupling over small ones [8]. Moreover, the fields that penetrate the tuning tubes fall off rapidly. Both the E and H-fields within the tuning tubes, normalized to their values at the tube openings, were simulated in CST and are shown in Fig. 3. As will be demonstrated, the cavity Q is very high despite the presence of a nearby lossy metal due to the field fall-off property and coupling region (the bellows conductivity is $7.75 \times 10^5\ S/m$).

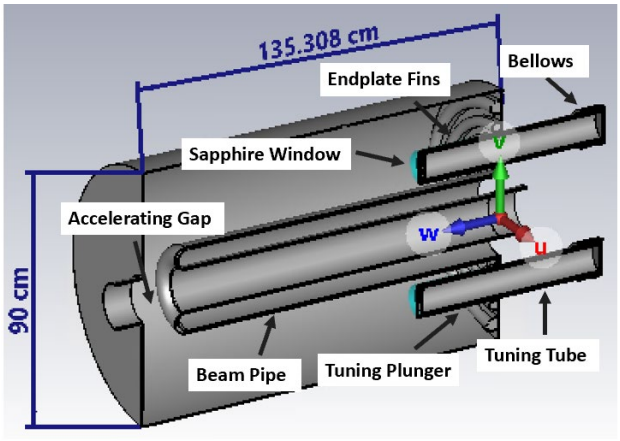

Fig. 1. Cutaway of proposed quarter-wave superconducting cavity.

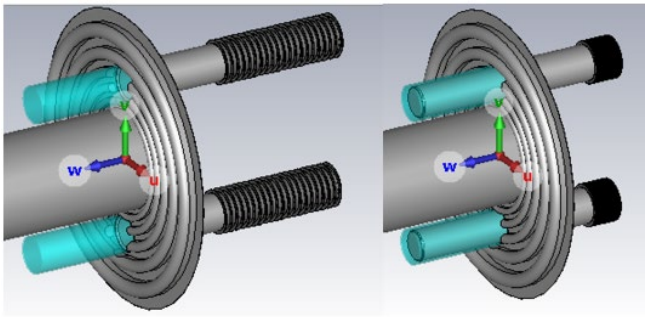

Fig. 2. Plunger tuning positions at full retraction (left) and full insertion (right).

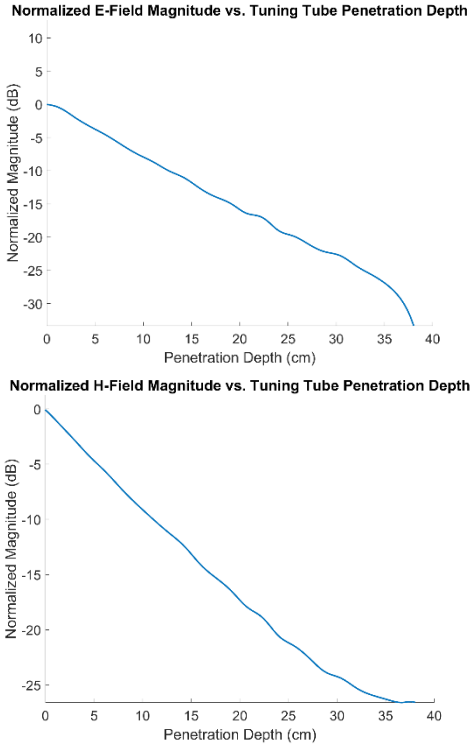

Fig. 3. Simulated normalized E-field (top) and H-field (bottom) magnitudes within the tuning tubes as a function of the penetration depth distance from the cavity-side opening.

TABLE I
PROPOSED CAVITY PARAMETERS AND RESULTS

Frequency	52.463 - 53.269 MHz
Unloaded Q	4.5 x 10^9 – 7.4 x 10^9
Cavity Diameter	90 cm
Cavity Length	135.1 cm
Beam Aperture	15.3 cm
Accelerating Gap	12 cm
Tuning Tube/Bellows Length	40-70 cm
Plunger Diameter	10 cm
Plunger Length	69 cm
R_s/Q (constant across range)	100 Ω
E_{acc} (constant across range)	18.33 MV/m
E_{pk}/E_{acc} (worst case)	3.15
B_{pk}/E_{acc} (worst case)	6.33 mT/MV/m
Heat Load at Max Gradient	21.9 W
Cryogenic Power Dissipation	16.67 kW
Loaded Q	2.5 x 10^4

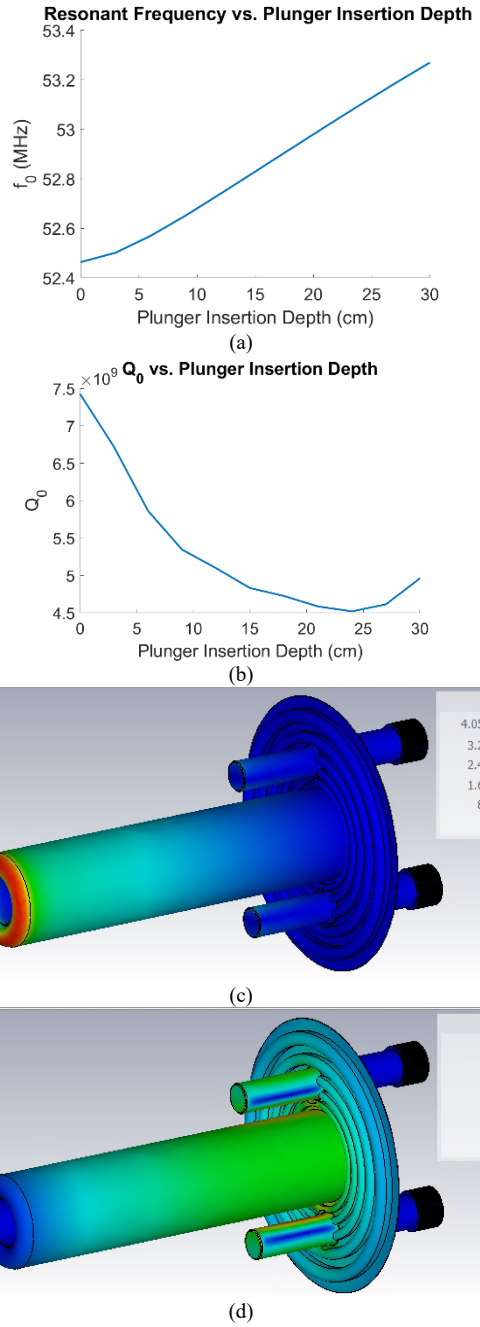

Fig. 4. Cavity fundamental mode resonant frequency (a) and unloaded Q as a function of plunger insertion depth (b), surface E-field distribution (c), and surface H-field distribution (d). Sapphire windows were hidden to show fields on niobium surfaces. Note the peak values are for a 1.4 MV/m gradient, as CST normalizes the fields to a strength where 1 J of energy is stored within the simulation space. All surface fields must be scaled accordingly for other gradient values.

Table I and Fig. 4 show the design parameters and resulting cavity fundamental mode properties obtained from eigenmode simulations in CST Microwave Studio assuming a 3 nΩ niobium surface resistance that is minimally affected by Q-slope decay and is dominated by the residual resistance given the low frequency [12]. Note that the loaded Q was computed from the beam-loaded circuit assuming a 2.11 A beam current, which is the operational value for the MI [13].

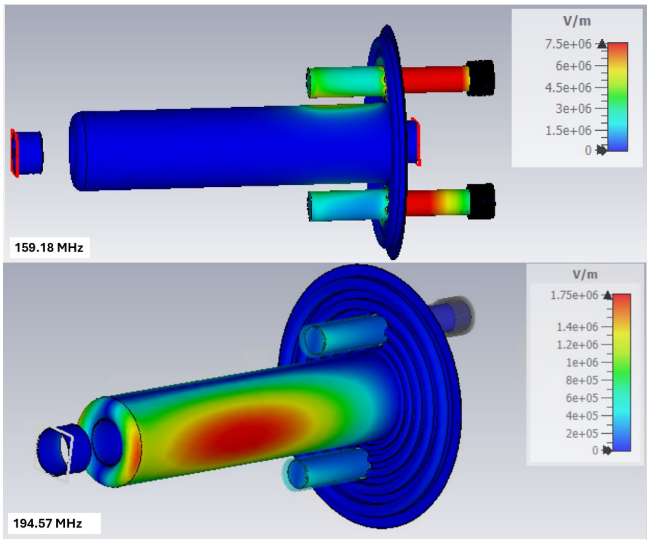

Fig. 5. Non-TEM parasitic HOM E-field distributions. Mode 3 (top) exists primarily on the plungers within the tuning tubes and mode 4 (bottom) is a higher-order coaxial mode. All modes of this type are non-accelerating.

TABLE II
PARTIAL HOM PARAMETERS

HOM Number	Frequency (MHz)	Mode Type	Q	R/Q
2	156.79	TEM	2×10^5	34.53
3	159.18	Plunger	783.80	.0117
4	194.57	Non-TEM	2.5×10^{10}	6×10^{-7}
5	238.79	Plunger	2183.66	.0113
6	254.76	TEM	5.74×10^6	18.36
7	265.44	Non-TEM	1.47×10^9	1.8×10^{-4}

Note also that for the cryogenic results, we assume a cavity unloaded Q of 2×10^9 (to obtain a more conservative estimate) and a temperature of 2 K in a cryomodule with 70 K and 5 K high and low temperature thermal shields each having static heat loads of 75 W and 25 W respectively (these heat loads are exaggerated estimates using Fermilab PIP-II SSR1 cryomodule data neglecting the support post and wire leads), and a cryoplant that can achieve 26% of the Carnot efficiency, which is consistent with the lower end of state-of-the-art facilities currently in operation [14], [15]. This captures all cryogenic subsystem efficiencies for the cryomodule, compressors, etc. to get a realistic wall-plug power estimate. As the results show, this design achieves the MI tuning range at plunger insertion depths between 15 and 25 cm. Note that the Q is not optimized for the 52.813 MHz to 53.104 MHz range, which was a deliberate choice to show the robustness of the performance; the cavity parameters (most notably Q and peak surface fields) remain in a favorable range even at significant insertion depths. This indicates that the performance limit of the plunger tuning technique is far beyond what has previously been reported.

The higher-order modes (HOMs) were also investigated, with the frequencies and metrics of a portion of them shown in Table II. Because of the cavity geometry and presence of the tuning tubes, several parasitic non-TEM modes appear in addition to the expected odd-order harmonic TEM coaxial modes characteristic of a quarter-wave cavity. Modes 3 and 4 in Table II are examples of such modes. Their E-field distributions are illustrated in Fig. 5. Note that these modes are degenerate, so each of them has at least one sister mode at the same or similar frequency with a field orientation that is mirrored or rotated about z-axis (w-axis in CST coordinates). As demonstrated in Table II, however, the R/Q values of the parasitic modes are exceptionally small, which means that, if excited, they will not interact with the beam. In any case, high-pass filtering HOM damping strategies have been implemented in the cavity reported in [2], which again, is very similar in style to the cavity presented herein. As such, the HOM performance of the proposed cavity does not present any challenges that have not already been overcome in the community. It is clear, then, that the RF performance of the presented design is sufficient for MI operation. However, the required tuning speed, repeatability, and precision still pose open questions for this scheme. Fortunately, commercial actuators exist that can meet these requirements. This will be discussed in more detail in the following section.

III. MECHANICAL ASPECTS OF TUNING

In this section, we will examine the feasibility of the proposed cavity design from a mechanical perspective. Specifically, we will show that the mechanical technology necessary to operate the cavity concept in the MI currently exists. We will first discuss the estimated kinematic requirements of the proposed topology as well as off-the-shelf actuator systems capable of meeting these requirements. Next, we will detail the bellows design and operation, paying special attention to aspects like bellows lifetime.

A. Actuator Kinematic Requirements

We will now estimate the required actuator specifications to achieve the nominal 1.2 s MI tuning cycle. This cycle will be the focus of this study instead of the faster ACE cycle in the interest of simplicity, though the proposed technique is scalable and the technology readily exists to double the speeds shown in the calculations below. The plungers shown previously are .1 m in diameter and .69 m in length. Let the plungers be hollow niobium with a 2 mm wall thickness, weighing 4 kg each. For this exercise, let the rest of the tuning assembly constitute no more than 6 kg of additional effective movable mass. During the MI cycle, the cavity will need to move across its 52.813-53.104 MHz tuning range and reset during a cycle similar to the one outlined in Fig. 2.5-2 of [15]. Fig. 6 shows a portion of the particle and plunger dynamics associated with this ramp. This figure shows that the maximum particle acceleration occurs ~.125 s into the cycle and amounts to 0.105 c/s (c is the speed of light). Since the cavity must follow the particle β, the frequency must be changing at a rate of ~5.5 MHz/s at this time. From the 3 MHz/m tuning slope determined from Fig. 4a, this corresponds to a maximum plunger velocity of 1.854 m/s. Let the plunger accelerate uniformly from 10 rest to 1.854 m/s beginning .075 s into the cycle, which requires 370 N of force for a 10 kg load. Note that RF drive is not applied until .1 s into the cycle, so plunger motion may begin during this time without issue, though we do not wish to accelerate the plunger during

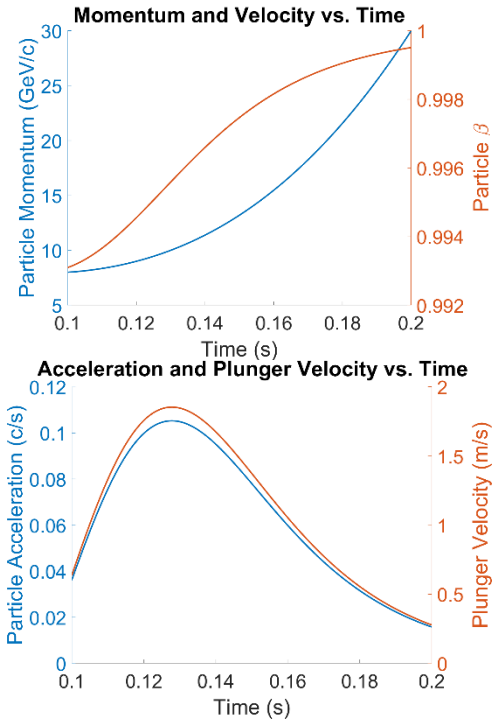

Fig. 6. 0.1 s snapshot of the MI H^- particle ramp (top) with particle acceleration and plunger velocity (bottom).

that entire time in order to minimize the total required bellows stroke (more on this below). Once the plunger reaches its maximum speed, it will slow down thereafter and be nearly halted when the momentum ramp ends, allowing the plunger to easily reset its position in < .5 s. This force estimate is aggressive since the cavity tuning range shown above is significantly larger than necessary, meaning the final plunger design may be shorter and thus lighter. Moreover, it may be possible to alter the ramp timing and RF drive pulse to achieve the nominal particle energy gain while reducing the plunger acceleration demand, which would be helpful but not required. Therefore, the 370 N estimate may be taken as a reasonable value.

B. Actuator Device

A potential actuator that can meet the requirements specified above is the PI (Physik Instrumente) V-857 High-Speed Linear Stage, which is a cost-effective linear motor system with a movable platform. For this study, a tuning rod connected to the plunger assembly would extend out of a light mounting block that is mechanically affixed to the movable platform, as is illustrated in Fig. 7. This actuator has a maximum drive force of 420 N, a maximum speed of 5 m/s, a travel range of 40 cm, a position resolution of 1 nm, a bidirectional repeatability of ± .5 µm, and a mean time before failure (MTBF) of 20,000 hr. The actuator exceeds the estimated max force requirement with a >10% margin, making it a safe choice for this initial study. Moreover, stronger, more expensive off-the-shelf motors are available if needed, with Hiwin and STXI Motion offering linear motors that can achieve peak forces in the kN range and speeds > 4m/s, which is enough to achieve the speed target of ACE. Therefore, the technology is available to readily adapt the

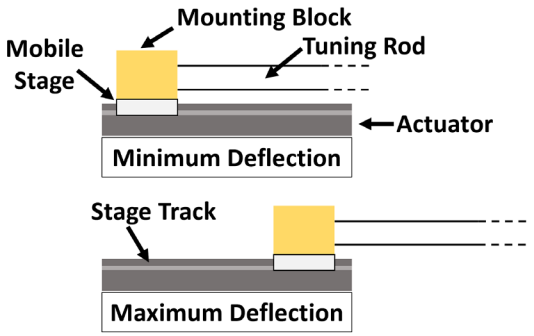

Fig. 7. Linear stage actuation diagram.

presented tuning technique to support faster ramp rates and larger tuning loads. Note that the PI V-857 actuator's stage position repeatability of ± .5 µm translates to a frequency error of ± 1.5 Hz, a negligible error for the MI use case. While usual superconducting applications require extreme levels of resonant frequency precision due to extremely high loaded Q values, the MI does not share this requirement. This is because the beam current in the MI is over 2 A. With this current, the beam loaded effective impedance of the cavity is low enough such that the design loaded Q is on the order of 10^4 as shown in Table I, negating the need for extreme actuator precision and alleviating microphonics/Lorentz Force detuning concerns as well. As such, this actuator is a feasible choice for meeting the specified tuning requirements for this study.

C. Cavity Vessel Interface

As shown above, the cavity concept proposed here includes edge-welded bellows as well as sapphire windows. The bellows are necessary, as the linear actuators need to operate outside of the helium vessel and must couple to the plungers via flexible hardware. This means there must be at least one bellows part per actuator. In Figs. 1 and 2, the tuning tubes are terminated with bellows, but the helium vessel is not shown. If the helium vessel were included, a second set of bellows would be attached to the helium vessel wall and an interfacing rod would couple between the bellows for each plunger, eventually connecting to the actuator block through thermal transitions in the cryomodule. Alternatively, since the tuning tube field coupling is so low, one could remove the bellows terminating the tuning tubes and allow helium to flow along both the plunger inner and outer surfaces, remaining isolated from the cavity inner volume due to the sapphire windows. This is viable since a) the plunger surface E-fields are low, mitigating the possibility of field emission, and b) the loss tangent of liquid helium is $< 10^{-10}$, so it will not affect the RF performance of the cavity if it enters the electromagnetic volume. Both implementations are illustrated in Fig. 8.

D. Bellows Lifetime and Redundancy

Under ideal conditions, the current Main Injector runs continuously during a 9-month period after which the machine is serviced during a 3-month shutdown. This constitutes ~20 million cycles under current MI operation and ~36 million under ACE. To accomplish this many cycles without bellows

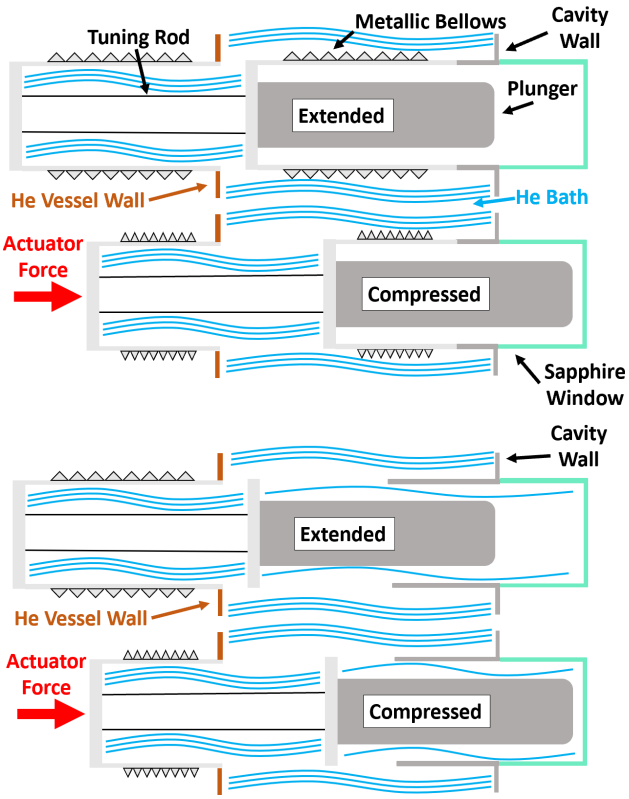

Fig. 8. Tuning assembly with four bellows (top) and with two bellows (bottom). Note that in the former configuration, the sapphire windows are not required. In the latter configuration, helium is allowed to enter the tuning tube and cavity volume, but it is isolated from the high E-field region of the cavity by the sapphire windows.

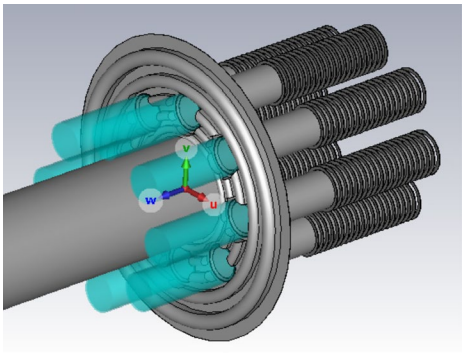

Fig. 9. Plunger redundancy scheme. Only two plungers need to be active at once.

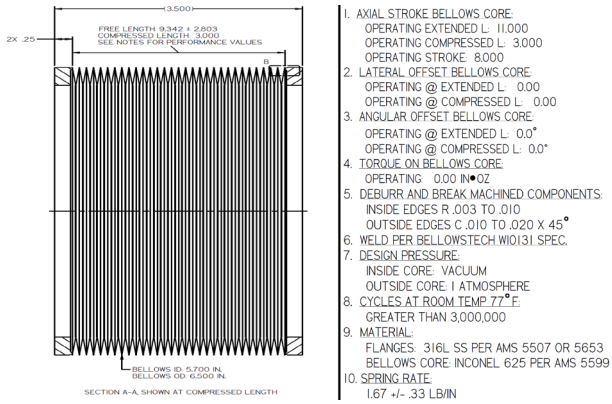

Fig. 10. Edge-welded bellows diagram (left) and performance specifications (right).

failure, a plunger redundancy scheme may be used, as shown in Fig. 9. Only two plungers need to be operational at one time, so when one plunger pair reaches its limit, another pair may take its place immediately. Because the inactive plungers couple to the cavity fields very weakly, and because of the field fall-off discussed above, the redundant plungers do not degrade the cavity Q to an unacceptable value; the worst case Q over the tuning range under this condition is 2.33 x 10^9. This staggered operation approach effectively reduces the bellows cycle lifetime requirement to 4-5 million for the current 1.2 s MI operation. At the request of the author, the industry provider MW Components has designed and quoted a custom Inconel 625 edge-welded bellows part that is theoretically capable of consistently exceeding 5 million 20 cm-stroke cycles before failure (though ISO standards prevent the vendor from being able to guarantee a lifetime above 3 million cycles). Since only approximately half of the maximum stroke is needed for the MI, this lifetime will be exponentially higher for the proposed mode of operation. Portions of the quoted bellows datasheet are shown in Fig. 10. While the bellows parts are consumable, they are inexpensive compared to the rest of the yearly operating costs of the Main Injector.

To achieve the ACE cycle requirements, plunger redundancy may be combined with cavity redundancy. Only 3 cavities are required to achieve the ACE gradient if they are run at 18.33 MV/m, but more may be implemented and placed on standby. In a similar manner as the plungers, the cavities may switch out to prevent overstressing the bellows.

The cavities on standby need not be powered and may be outfitted with reconfigurable Q-spoiling dampers to limit beam perturbation.

While many other mechanical details must be examined to commission the proposed cavity, the elements described above establish a solid baseline to conclude mechanical feasibility of the tuning scheme. In the next section, results will be shared detailing the multipacting performance of the cavity.

IV. Multipacting Simulations

Multipacting mitigation is a critical element of SC cavity design, as resonant electron excitation can easily quench a cavity if it is not abated [12]. As such, multipacting simulations were conducted for the proposed cavity and structural modifications were made to prevent potential resonances. Two CST Particle Studio solvers were used to conduct this study; the Particle Tracking solver and the Particle-In-Cell (PIC) solver. The Particle Tracking solver was run first as a preliminary simulation to diagnose problem sites in the cavity geometry and test mitigating strategies. Then, the PIC solver was used to stress the structure with a much larger number of primary electron emissions to confirm multipacting immunity. Fields were imported from the Eigenmode solution for use in the particle simulations. For this study, simulations were conducted with two plungers fully inserted into the cavity without sapphire windows, allowing for examination of their worst-case effects.

For the Particle Tracking simulations, particle sources were defined on the outer conductor (792 emission points), the center

conductor (1008 emission points with 814 on the rod and 194 on the curved end), the endplate on the shorted end of the cavity (334 emission points), and both plungers (120 emission points per plunger). The emission points were distributed via a triangular grid across the source surfaces. An example emission point distribution is shown in Fig. 11. Note that the tracking simulation was conducted at full gradient (18.33 MV/m). To simulate the niobium Secondary Electron Yield (SEY) characteristics, the Furman Model for argon discharge-cleaned niobium was used [17]. The true SEY curve for this model is shown in Fig. 12.

Fig. 13 illustrates the trajectory results of the particle tracking simulation without the fin structures on the shorted endplate. The zoomed-in portion of the figure highlights several locations where it appears that secondary emission resonances are occurring (the thick sections of trajectory threads signify several multi-point multipacting instances). Based on the simulation results, the endplate is the only location likely to multipact, which was unexpected based on the multipacting results given in [18]. The authors of that work observed multipacting at locations closer to the accelerating gap, whereas no such multipacting is indicated here. This is likely due to the lower center-to-outer conductor diameter ratio of the cavity presented in this work, which allows emitted electrons more space to accelerate before impacting a surface, but not so much space as to create higher-order resonances, lowering the likelihood of secondary emission.

To deal with the multipacting at the shorted end, 5 raised half-toroidal fins were added to the endplate, scaling up in size as the outer conductor is approached. Much in a similar manner as the strategy deployed to mitigate multipacting in [18], these fins are designed to disrupt the resonant particle paths. The smallest, innermost fin has an inner radius of 16.5 cm and an outer radius of 18.5 cm. The distance of the toroidal center of the fin and the endplate is 1 cm. The rest of the fins were modeled by scaling the innermost fin repeatedly by a factor of 1.22. This geometry is shown in Fig. 14. Once the fins were added, the Particle Tracking simulation was repeated. The new trajectories are shown in Fig. 15. Zooming in once more, we see that the multipacting resonant sites have been eliminated. While there is still some trajectory clustering near the plunger penetrations, these do not lead to runaway multipacting behavior, as we will see.

We are now prepared to move to the PIC simulations, which can introduce hundreds of thousands of primary electrons to the simulation space and track their existences for long time periods. For these simulations, the 300°C bakeout treatment Furman model shown in [17] was used for the SEY characteristics instead of the discharge-cleaned data, as this presents less favorable SEY values, and thus a more conservative multipacting estimate. This model is shown in Fig. 16. The particle sources for the PIC simulations were placed on the same surfaces as for the Particle Tracking simulations, though with somewhat fewer emission sites per surface in the interest of simulation time. Here, the outer conductor had 460 emission sites, the center conductor had 530, the plungers had 120 per plunger, and the finned endplate had 678. Unlike with the tracking solver, the primary emission from the particle sources can be controlled as a function of time in the PIC solver.

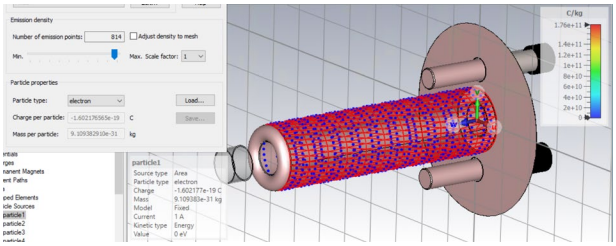

Fig. 11. Example particle source distribution on cavity center conductor.

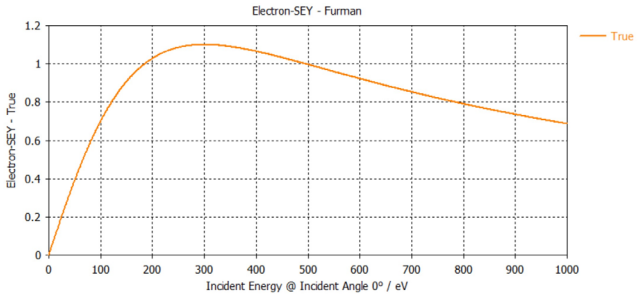

Fig. 12. Furman model True SEY for Particle Tracking simulations.

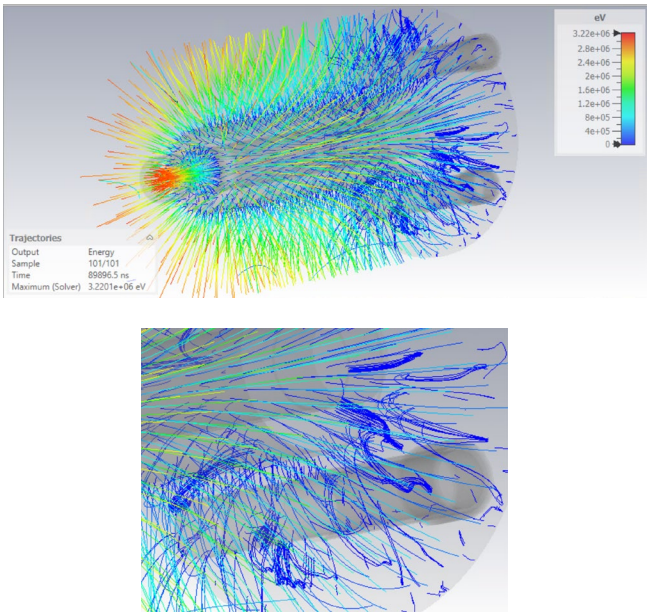

Fig. 13. Particle Tracking simulation trajectories of cavity without endplate fins (top) and zoomed-in view of resonant trajectories at the endplate (bottom).

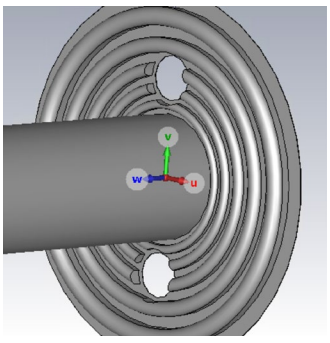

Fig. 14. Endplate multipacting mitigation fins with plungers hidden. Note there is a 10 mm clearance between the plunger surfaces and the fins.

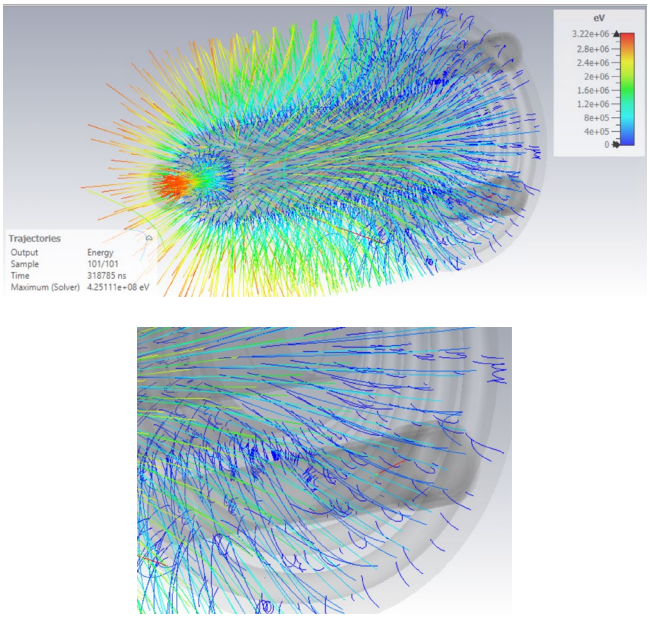

Fig. 15. Particle Tracking simulation trajectories of cavity with endplate fins (top) and zoomed-in view of trajectories at the endplate to show resonance mitigation (bottom).

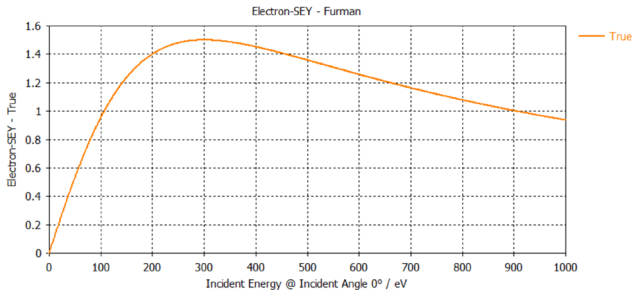

Fig. 16. Furman model True SEY for PIC simulations.

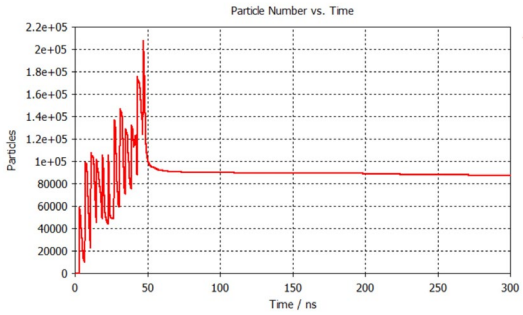

Fig. 17. PIC simulation particles emitted from sources.

Using this feature, we can ensure that multipacting is mitigated regardless of at what RF phase the primary electrons are emitted. For these simulations, primary electrons will be emitted in 12 equal Gaussian bunches, each spaced 4 ns apart or approximately 1/5 of an RF period at 53 MHz. The particle bunches are kept narrow ($\sigma = .015$ ns) so that multipacting, if occurrent, can be narrowed down to a particular region of RF phases. While it is not possible to control the exact number of particles per bunch, each bunch constitutes upwards of 60,000 electrons. Fig. 17 shows the particle evolution within the simulation space as a function of time due to just the particle sources (any particles that impacted a surface were absorbed with no secondary emission).

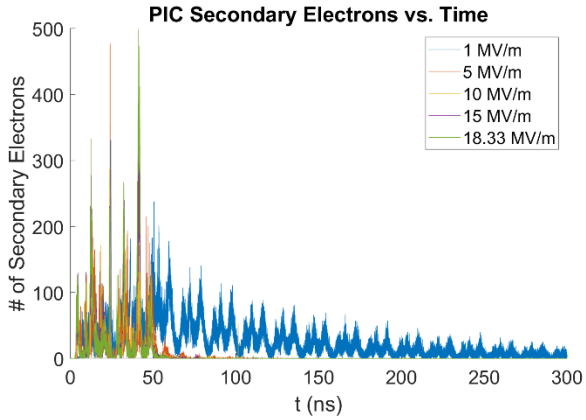

Fig. 18. Secondary emission PIC simulation results at varying gradients.

Note that the particles left over at the end of the simulation are likely trapped in the simulation space and simply have not impacted any surfaces by the time the simulation has ended. The spiked nature of the particle count does however indicate that many impacts are occurring, so the leftover particles are not an issue.

To examine the multipacting thoroughly, a PIC simulation was conducted at multiple gradient strengths and the number of emitted secondary electrons was plotted as a function of time. The secondary electron curves are illustrated in Fig. 18. As the curves show, the secondary electron emission is minimal for multiple gradients between 1 MV/m and 18.33 MV/m. Given the large number of primary particles, this indicates that a) the endplate fin implementation was effective and b) no other major multipacting sites exist. Given these results, it is safe to conclude that multipacting will not be a limiting factor for the implementation of the proposed cavity topology.

V. Conclusion

In this work, we have developed and presented a design concept for a broadband mechanically-tuned superconducting cavity that is appropriate for implementation in the Fermilab Main Injector. The cavity tuning mechanism expands upon the plunger insertion method and the required tuning speed may be readily achieved using existing hardware and actuator technologies. It has been shown that the cavity RF performance is on-par with that of typical SC cavities. It has also been shown that mechanical, cryogenic, microphonic, and multipacting considerations do not present insurmountable obstacles for the MI use case. As such, the design presented herein is worthy of further investigation and prototyping. This will be the subject of future research.

Acknowledgment

The author would like to thank Vyacheslav Yakovlev for introducing the idea to the author of investigating broadband superconducting cavity topologies. The author would also like to thank the FNAL RF department, as well as, in no particular order, Brian Chase, Alexander Valishev, Ding Sun, Bob Zwaska, Jeremiah Holzbauer, Paolo Berutti, Robyn Madrak, Paul Derwent, Jay Theilacker, and Gennady Romanov for helpful discussions.

REFERENCES

[1] S. Gori et. al., "ACE Science Workshop Report," arXiv preprint arXiv:2403.02422, March 2024.
[2] Q. Wu et. al., "Operation of the 56 MHz Superconducting RF Cavity in RHIC with Higher Order Mode Damper," In *Phys. Rev. Accel. Beams*, vol. 22, no. 10, p. 102001, October 2019.
[3] S.A. Belomestnykh, et. al., "Tunable 28 MHz Superconducting Cavity for RHIC," In *Proc. 3rd International Conference on Particle Accelerator (IPAC 2012)*, 2012, pp. 2405-2407.
[4] N. Shipman, et. al., "A Ferroelectric Reactive Tuner for Superconducting Cavities," In *Proc. 19th Int. Conf. on RF Superconductivity (SRF 2019)*, 2019, pp. 783-790.
[5] G. Cavallari et. al., "The Tuner System for the S.C. 352 MHz LEP 4-Cell Cavities," In *Proc. 3rd Workshop on RF Superconductivity*, 1987, pp. 625-638.
[6] D. Boussard et. al., "The LHC Superconducting Cavities," In *Proc. 1999 Particle Accelerator Conference (PAC'99)*, New York, NY, 1999.
[7] S.V. Kuzikov and V.P. Yakovlev, "A Fast Mechanical Tuner for SRF Cavities", In *Proc. SRF'21*, East Lansing, MI, USA, Jun.-Jul. 2021, pp. 600-603.
[8] D. Longuevergne et. al., "An Innovative Tuning System for Superconducting Accelerating Cavities," In *Nuclear Instruments and Methods in Physics Research*, vol. 749, pp. 7-13, June, 2014.
[9] G. Olry, et. al., "Development of a Beta 0.12, 88MHz, Quarter-Wave Resonator and its Cryomodule for the SPIRAL2 Project," In *Physica C: Superconductivity*, vol. 441, Issues 1–2, pp. 197-200, July, 2006.
[10] T. Junquera et. al., "Design of a Superconducting 352 MHz Fully Jacketed Double-Spoke Resonator for the ESS-Bilbao Proton Linac," In *Proc. 16th Int. Conf. on RF Superconductivity (SRF 2013)*, 2013, pp. 929-932.
[11] P. Brown et. al., "Status of the LEP Accelerating Structure," In *Proc. 13th IEEE Accelerator Conference*, Chicago, IL, 1989.
[12] H. Padamsee, J. Knobloch, and T. Hays, *RF Superconductivity for Accelerators*, New York, NY: John Wiley & Sons Inc., 1998.
[13] T. Wangler, *RF Linear Accelerators*, Weinheim: Wiley-VCH Verlag GmbH & Co., 2008.
[14] The PIP-II Conceptual Design Report, United States, 2017, https://doi.org/10.2172/1346823.
[15] The Fermilab Main Injector Technical Design Handbook, United States, 1994, https://doi.org/10.2172/1127909.
[16] S. Yoon et. al., "SCL3 cryogenic plant process design for RAON," In *2019 IOP Conf. Ser.: Mater. Sci. Eng.*, 502 012009.
[17] G. Romanov, "Simulation of Multipacting with Space Charge Effect in PIP-II 650 MHz Cavities," In *Proc. North American Particle Accelerator Conference (NAPAC2016)*, Chicago, IL, USA, 2016, pp. 1142-1145.
[18] D. Naik and I. Ben-Zvi, "Suppressing multipacting in a 56 MHz quarter wave resonator", In *Phys. Rev. ST Accel. Beams*, 13, 052001, 2010.